ENGINEERING RESEARCH INSTITUTE
UNIVERSITY OF MICHIGAN
ANN ARBOR

STUDY, DEVELOPMENT, AND PRODUCTION OF FERROSPINELS

APPLICABLE TO TUNING OF SEARCH RECEIVERS

QUARTERLY PROGRESS REPORT NO. 1, TASK ORDER NO. EDG-6
Period Covering October 1, 1952 to December 31, 1952

Electronic Defense Group
Department of Electrical Engineering

By: D. M. Grimes
B. Hershenov
E. Katz
L. W. Orr
L. Thomassen
E. F. Westrum, Jr.
M. H. Winsnes

Approved by: H. W. Welch, Jr.
H. W. Welch, Jr.
Project Engineer

Project M-970

CONTRACT NO. DA-36-039 sc-15358
SIGNAL CORPS, DEPARTMENT OF THE ARMY
DEPARTMENT OF ARMY PROJECT NO. 3-99-04-042
SIGNAL CORPS PROJECT 29-194B-0

January, 1953

TABLE OF CONTENTS

	Page
TASK ORDER	v
ABSTRACT	vii
1. PURPOSE	1
2. PUBLICATIONS AND REPORTS	1
3. ORGANIZATION OF THE PROGRAM	2
4. FACTUAL DATA	2
4.1 Preliminary Check of the Theory of Reversible Susceptibility	2
4.1.1 Experimental Results	2
4.1.2 Experimental Methods	6
4.1.2.1 60-Cycle B-H Loop Plotter	6
4.1.2.2 Parallel Incremental Permeability Measurement	8
4.1.2.3 Transverse Incremental Permeability	10
4.2 The Basic Ferrospinel Components	14
4.3 The Manufacturing of the Ferrites	15
4.3.1 Manufacturing Procedure	15
4.3.2 Manufacturing Equipment	15
4.4 Magnetic and Electrical Measurements	16
4.4.1 Saturation Magnetization	16
4.4.2 Incremental Permeability, Dielectric Constant, Resistivity, and Power Losses in the Core Material	16
4.4.2.1 Resistivity and Dielectric Constant	16
4.4.2.2 Incremental Permeability	16
4.5 Applicable Physical Measurements	18
4.5.1 Density	18
4.5.2 Magnetostriction (no work done)	18
4.5.3 Thermal Expansion Coefficient (no work done)	18
4.5.4 X-Ray Diffraction	18
4.5.5 Metallographic Polishing	23
4.5.6 Curie Temperatures	24
4.5.6.1 Ferrimagnetic Curie Point	24
4.5.6.2 Antiferromagnetic-Ferrimagnetic Curie Points	24
4.5.7 Cryogenic Apparatus	25
4.5.7.1 The Cryostat	25
4.5.7.2 The Calorimeter	28
4.5.7.3 Electrical Circuits	31
4.5.7.4 Method of Operation	31
4.5.8 Measurement of the Hall Effect in Ferrites	32
4.5.9 Description of Apparatus for Measurement of Hall Effect	35
4.5.9.1 Driving Stage	35
4.5.9.2 The Detection Circuit	36
4.5.9.3 Bucking Section	36

Page

4.5.9.4 25 CPS Signal Generator 37
4.5.9.5 AC Magnet 37
4.5.9.6 Possible Revisions 37
4.5.10 Microwave Studies at Over 500 MC (no work done) 38
4.5.11 Thermal Conductivity (no work done) 38

5. CONCLUSIONS 38

6. PROGRAM FOR THE NEXT INTERVAL 38

6.1 Reversible Susceptibility 38
6.2 Oxide Purity 39
6.3 Core Manufacturing Equipment 39
6.4 Measurement of Magnetic and Electrical Properties 39
6.5 Applicable Physical Measurements 39

REFERENCES 40

DISTRIBUTION LIST 41

TASK ORDER

Title: STUDY, DEVELOPMENT, AND PRODUCTION OF FERROSPINELS APPLICABLE TO TUNING OF SEARCH RECEIVERS

Purpose of Task:

To further the development of ferrospinels of different incremental permeabilities and low losses, with reference to specific applications of interest to the Signal Corps such as RF tuning units.

Procedure:

The approach to the general objective will include:

a. The preparation, under controlled conditions, of specimens of of different compositions;

b. The measurement of parameters such as the incremental and initial permeabilities, the saturation inductance, the coercive force and the Q (figure of merit) at various frequencies;

c. The interpretation of these magnetic parameters in terms of the composition, reaction temperature, pressure and other conditions in the preparation of the samples;

d. The relationship of the solid state properties of the crystallite with the various measured magnetic parameters;

e. Theoretical explanations, where possible, for the relationships found in d. above.

Reports and Conferences:

a. Quarterly Task Order Reports shall be submitted reporting technical detail and progress under this Task Order;

b. Task Order Technical Reports of a final summary type are in general desirable and shall be prepared at the conclusion of investigations of each major phase. Such reports shall be prepared as

decided in conference between the Electronic Defense Group and the Contracting Officer's Technical Representative in the Countermeasures Branch, Evans Signal Laboratory.

Personnel:

Electronic Defense Group:

Project Physicist: Mr. D. M. Grimes

Countermeasures Branch, Evans Signal Laboratory:

Project Engineer: Mr. Leon I. Mond

Components and Materials Branch, Squier Signal Laboratory

Project Scientist: Dr. E. Both

Comments:

The classification of this Task Order as Unclassified shall not preclude the classification of individual reports according to the information they contain, as determined in conference with the Contracting Officer's Technical Representative.

M. KEISER
Chief, Countermeasures Branch
Contracting Officer's Technical
Representative

ABSTRACT

In this report the work now being done on permeability measurements, X-ray diffraction, metallographic polishing and etching, and specific heat measurements are described. In addition, the manufacture of ferrite samples is outlined. The other measurements which will be undertaken to determine the quality of the cores are listed.

STUDY, DEVELOPMENT, AND PRODUCTION OF FERROSPINELS APPLICABLE TO TUNING OF SEARCH RECEIVERS

QUARTERLY PROGRESS REPORT NO. 1
January, 1953

1. PURPOSE

The purpose of this report is to summarize the progress made by the Electronic Defense Group to further the development of ferrospinels of different incremental permeabilities and low losses, with reference to specific applications of interest to the Signal Corps, such as RF tuning units.

The work is being directed toward the objective of better ferrite cores as rapidly as possible. It is necessary, however, to take advantage of any particular tools which are accessible and utilize them, even though other measurements which must be set up seem of more importance. An example is the contrast of the measurement of the Hall coefficient and that of magnetostriction. Although the measurement of magnetostriction would, perhaps, give information of more immediate usage, the apparatus for the measurement of the Hall coefficient is at hand while that for magnetostriction is not.

2. PUBLICATIONS AND REPORTS

No publications were issued during the quarter on Task Order No. EDG-6. If equipment now on order arrives in time, a technical report will be prepared during the following quarter regarding the experimental verification of the theory of reversible susceptibility in ferrites issued previously under Task Order No. EDG-4.[1]

Mr. D. M. Grimes outlined the program in a paper entitled "Some Problems in the Solid State Physics of Ferrites" at the Electronic Defense Group Symposium held in Ann Arbor, November 20 and 21.

3. ORGANIZATION OF THE PROGRAM

There are, in addition to the Electrical Engineering Department, under whose auspices this contract was initiated, three departments of the University actively engaged in this research work. These departments are the Physics Department, the Chemical and Metallurgical Engineering Department, and the Chemistry Department. Representing these departments are Professors Katz, Thomassen, and Westrum, respectively.

Briefly, the program will be to obtain cores of desirable characteristics, to measure these characteristics, then to attempt to synthesize more cores with these same characteristics.

Some cores have been requested and received from Mr. Gerhard H. Dewitz of the C.G.S. Laboratories, Stamford, Connecticut. These cores represent some not acceptable to him and some of good quality. These cores will be analyzed to see if the differences can be localized and thus, hopefully, controlled.

4. FACTUAL DATA

4.1 Preliminary Check of the Theory of Reversible Susceptibility (D. M. Grimes, E. Katz, L. W. Orr, M. H. Winsnes)

4.1.1 Experimental Results. The results quoted herein are accurate to no more than 5%, and are preliminary results based upon one measurement only.

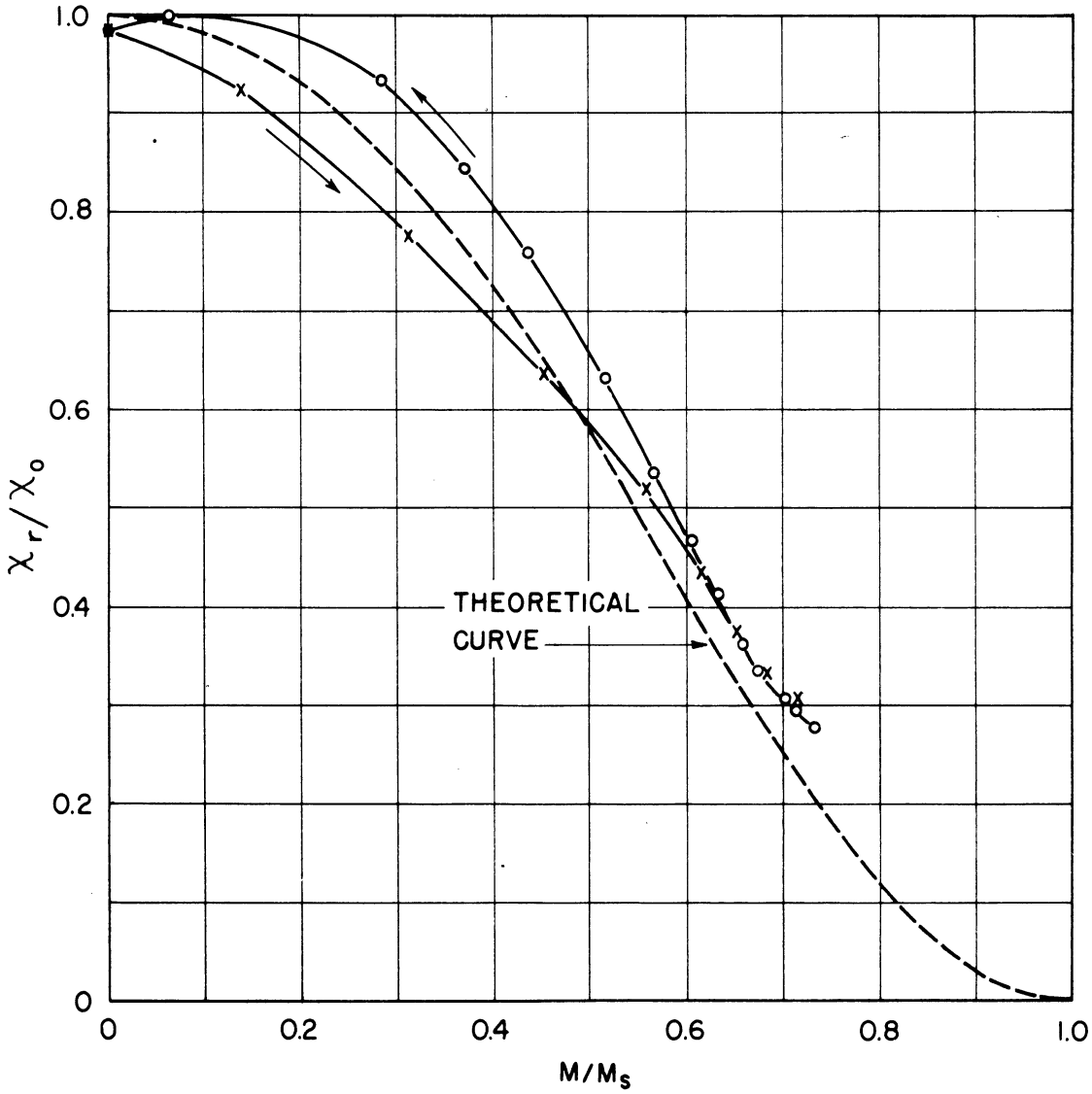

GC-E-3

REVERSIBLE SUSCEPTIBILITY; PARALLEL FIELDS

FIG. 1

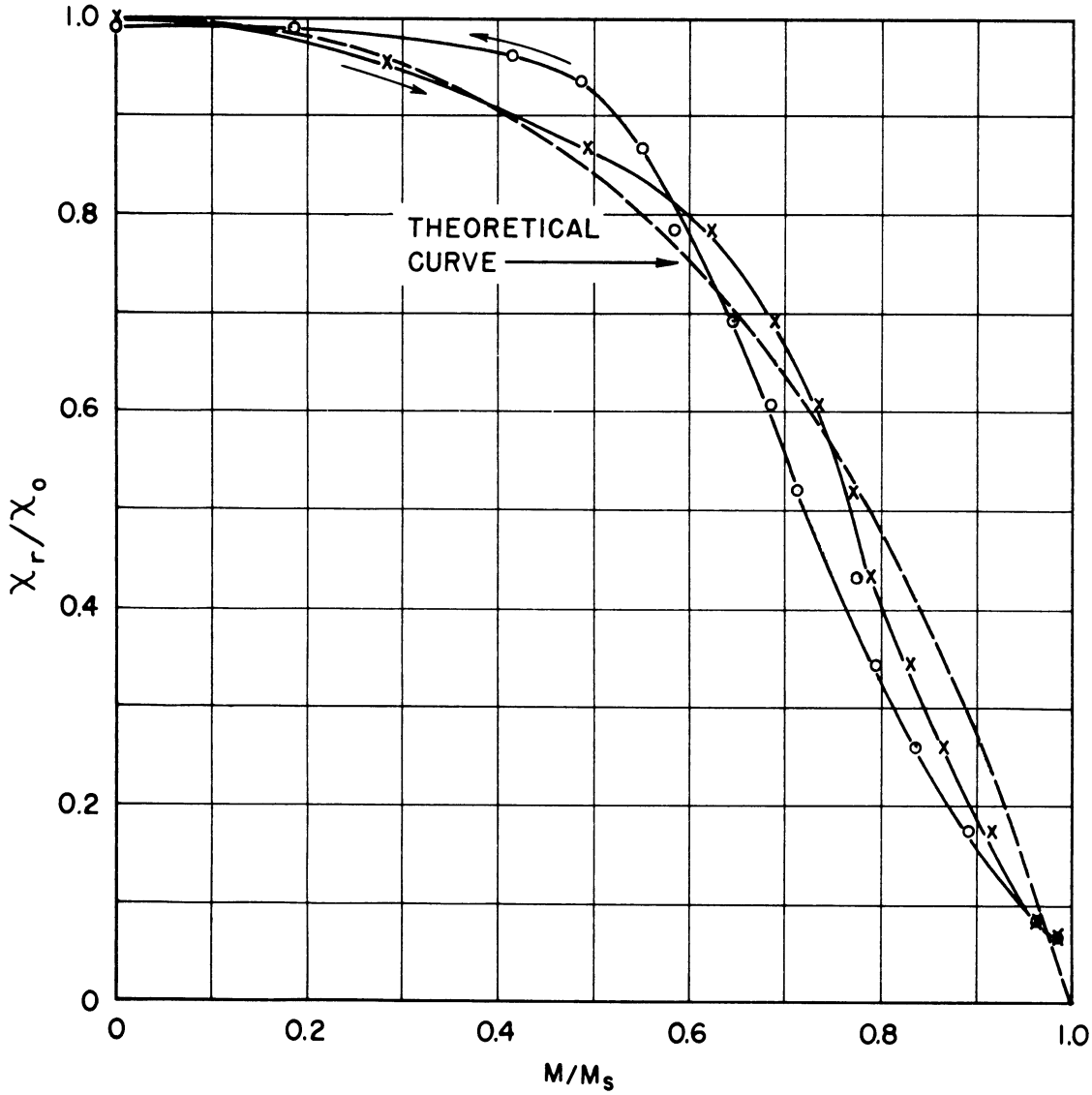

GC-E-3
REVERSIBLE SUSCEPTIBILITY; TRANSVERSE FIELDS.

FIG. 2

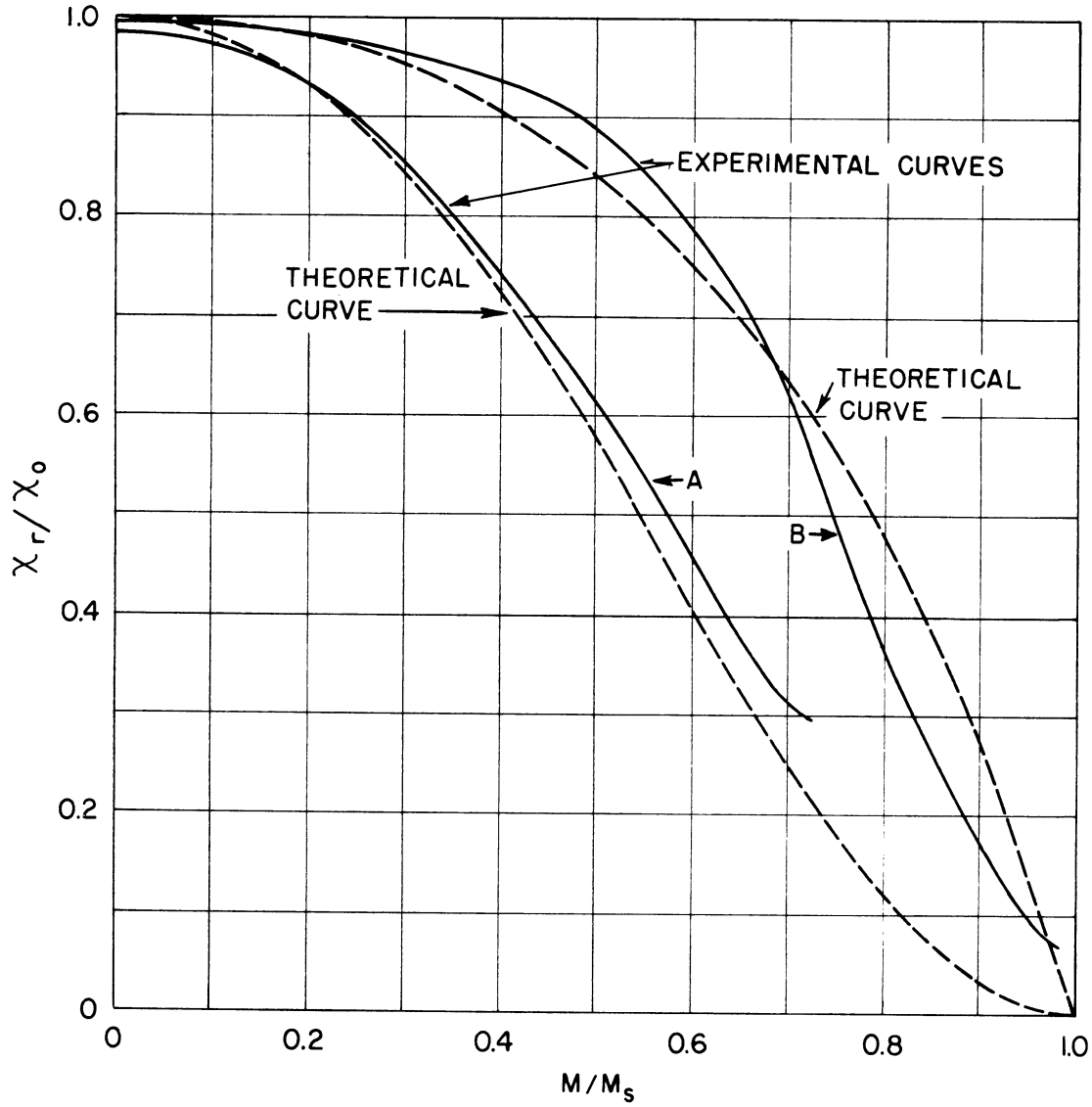

GC-E-3

REVERSIBLE SUSCEPTIBILITY;

CURVE A - PARALLEL FIELDS

CURVE B - TRANSVERSE FIELDS.

FIG. 3

More extensive measurements are under way. The susceptibility temperature dependence will also be studied.

The theoretical curves were developed in reference 1. The method of obtaining the experimental curves will be described in the following sections.

Figs. 1, 2, and 3 show graphically the results. Fig. 1 is for parallel biasing and incremental fields; Fig. 2 is for transverse biasing and experimental fields. Fig. 3 shows the average experimental curve plotted against the theoretical value in both cases. The agreement is quite satisfactory.

4.1.2 Experimental Methods

4.1.2.1 60-Cycle B-H Loop Plotter. Preliminary attempts to check the theory of reference 1 was done by plotting a 10 kc B-H loop. It was found that the value of the coercive force decreased rapidly with decreasing frequency. To correct this a 60-cycle B-H loop plotter was built. The circuit is shown in Fig. 4, and consists of four main components:

a. The test core, equipped with B and H windings of 100 turns each.

b. A direct coupled integrating amplifier (V_1 and V_2) powered by a voltage-regulated power supply (V_3, V_4, V_5, and V_6).

c. A variac T_1 and transformer T_2 to furnish driving current to the H circuit.

d. An oscilloscope to display the 60-cycle B-H loop.

The integrating amplifier is necessary at this operating frequency to degenerate the internal noise to a low value, while at the same time giving a good integration at 60 cycles. The "integration error" of the amplifier is less than 1% at 60 cycles.

The output of the amplifier is connected to the Y input of the

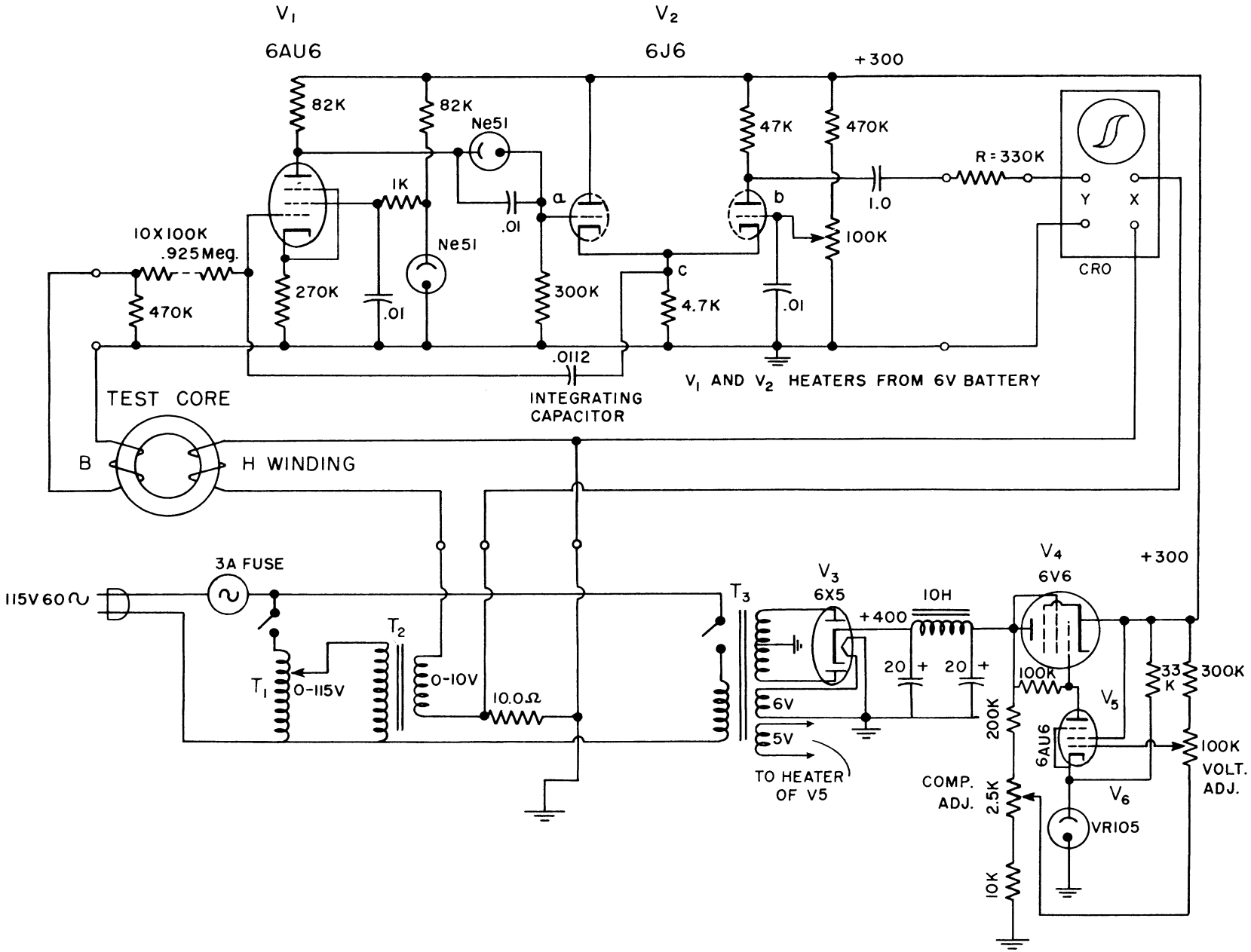

FIG. 4

CIRCUIT OF 60 CYCLE B-H LOOP PLOTTER.

oscilloscope. The output voltage is given by

$$e_o = k \int_o^t e_i \, dt \quad .$$

where e_i is the input voltage from the B winding, and k is the integrating amplifier constant. Oscillograms may be calibrated by a method similar to the one outlined in reference 4. In this case, however, the constant k must be determined, and this is most accurately found by experiment.

The theory of operation, circuit details, and method of calibration will be fully described in a technical report to be issued shortly under Task No. EDG-4.

4.1.2.2 Parallel Incremental Permeability Measurement. A revision was made in the previous circuit, Fig. 9 of reference 4. The new circuit has no switching transients, but has the disadvantage of requiring two H windings. One cycle of bias field variation takes more than ten seconds, and there is no detectable signal picked up in the B winding due to the variations in H_o.

The circuit of the revised equipment is shown in Fig. 5. The operation of the circuit is as follows:

The 6SL7 multivibrator circuit charges and discharges the 1 mfd condensers in the 6L6 grid circuits at a slow rate, and alternately drives the 6L6's to conduction and cut-off. The result is that current is flowing alternately in the two H windings. The two H windings indicated in Fig. 5 are on the test core. The B winding is not shown. The H_1 and H_2 windings are arranged so they give rise to opposite magnetic fields. The effective field is a function of the difference current through the two windings. Terminals A and B in Fig. 5 are connected to the X-input of the scope and the X displacement therefore indicates the net biasing field H_o.

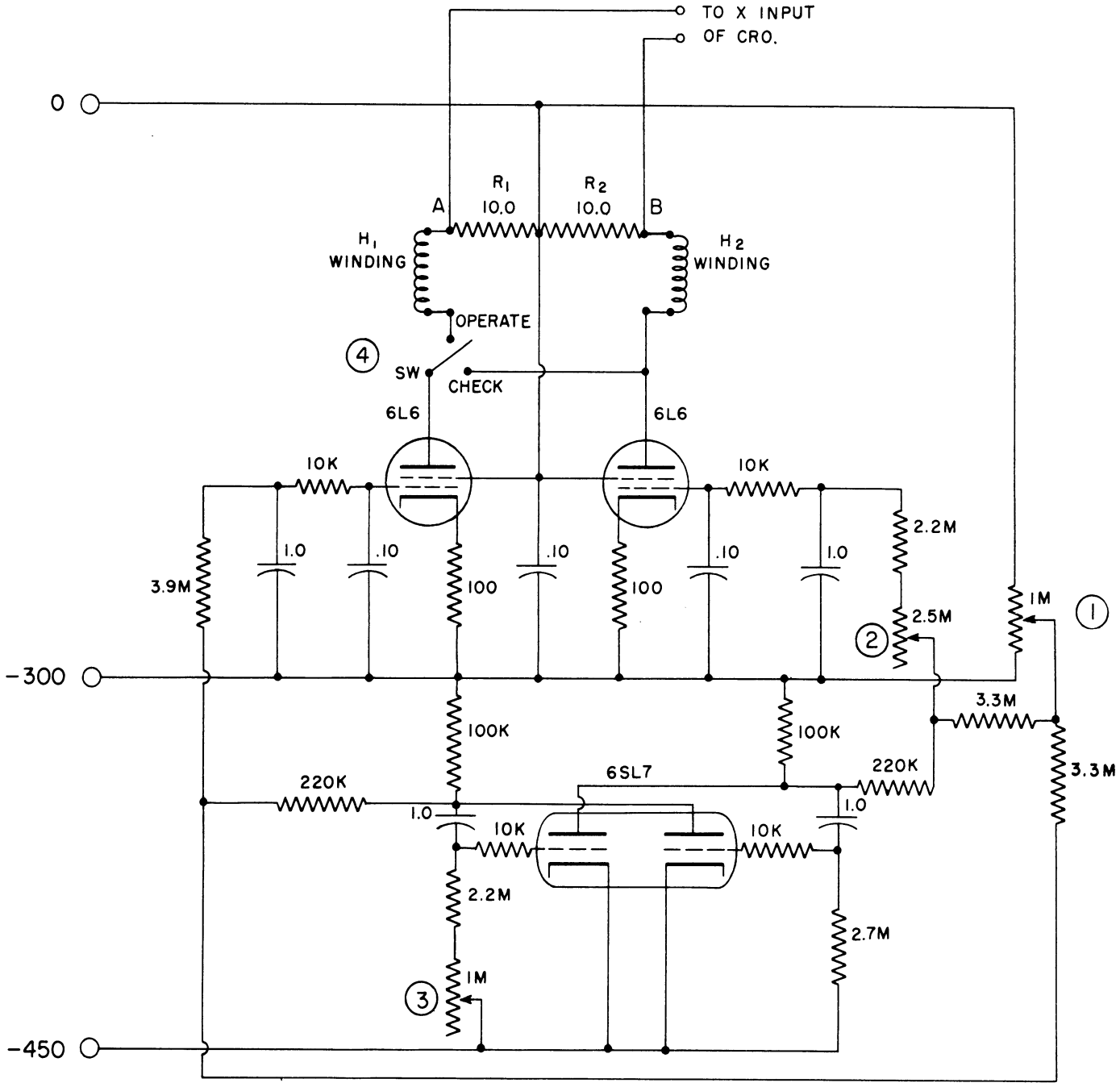

① H MAX. (BIAS)

② H+MAX. = H− MAX.

③ SYMMETRY T− = T+

④ SWITCH FOR H+M = H−M CHECK AND ONE WAY PLOT.

FIG. 5

REVISED DRIVE CIRCUIT OF THE BUTTERFLY LOOP PLOTTER.

The B winding is driven from an oscillator through a 10,000 ohm series resistor. When the impedance of the inductor is much smaller than 10,000 ohms, the ac current through the windings is not a function of H_o. When this current is small and the frequency relatively high, the incremental permeability is proportional to the voltage across the B winding. This voltage is plotted vertically on the scope. The envelope of the scope pattern is a μ - H butterfly-loop. More detailed discussion of the circuit will be given in the subsequent technical report.

4.1.2.3 Transverse Incremental Permeability. An oscilloscopic picture of $\mu_{\Delta t}$ vs B can be made by the apparatus illustrated in Fig. 6 and consists of the following:

a. The test core has an interior and exterior girdle winding, as well as a 200-turn tapped toroidal winding, which is wound continuously from 0° to 360° on the core and tapped at 90° and 180°. The wire is then wound in the same direction from 360° back to 0° so that none of the 60-cycle transverse field is coupled into the 200-turn winding. (See Figs. 7 and 8.)

b. A 60-cycle integrating amplifier (see Fig. 4) and oscilloscope to display the vertical flux density as well as variation in permeability.

c. A 60-cycle uniform magnetic field to drive the specimen.

d. An oscillator driving the toroidal winding to produce the incremental permeability-measuring signal.

The operation of the apparatus is as follows: first the toroid core has to be oriented perpendicular to the 60-cycle magnetic field, so there is no 60-cycle flux flowing tangentially in the toroid. This means that the toroid has to be oriented so there is no 60-cycle signal developed in either quadrant of the 200-turn winding.

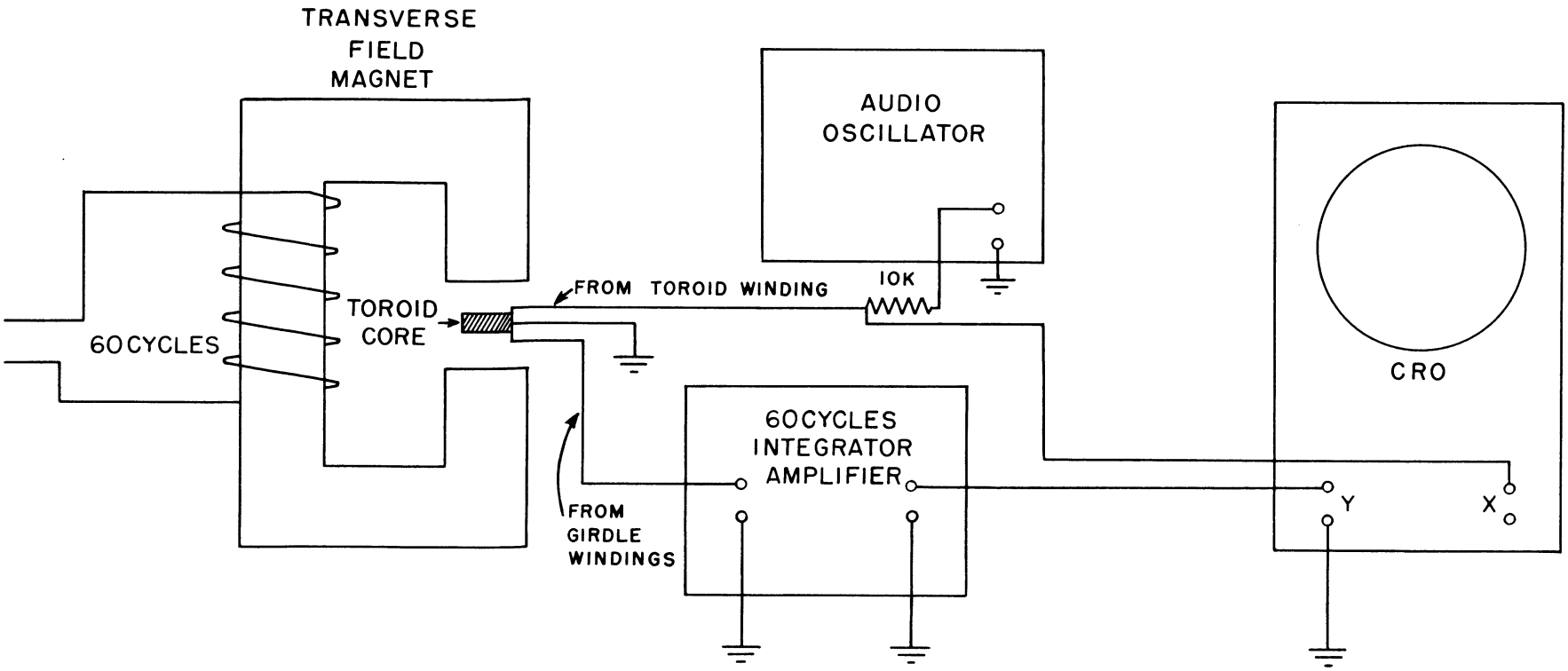

FIG. 6

TRANSVERSE PERMEABILITY PLOTTER.

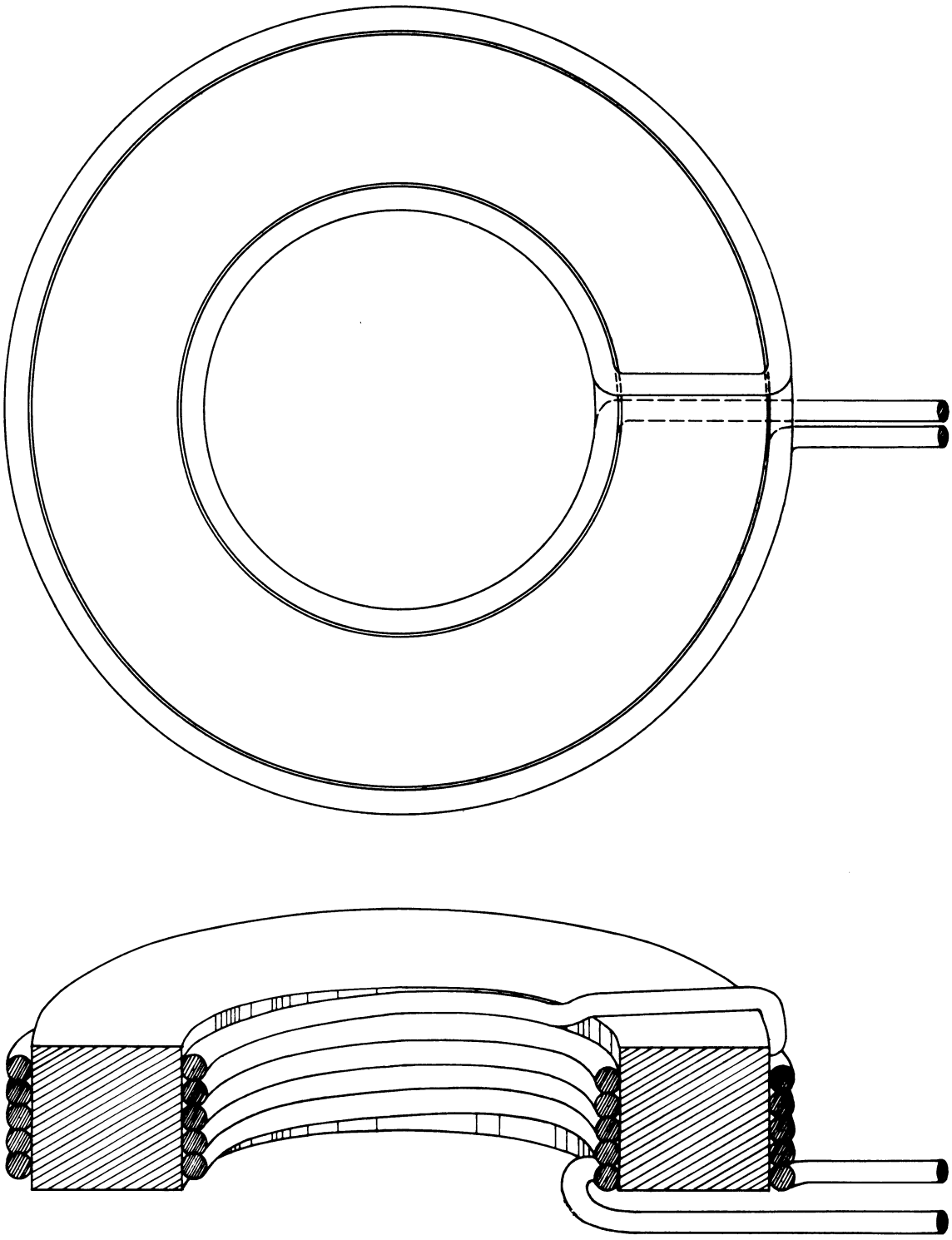

FIG. 7

TOROID SHOWING GIRDLE WINDINGS.

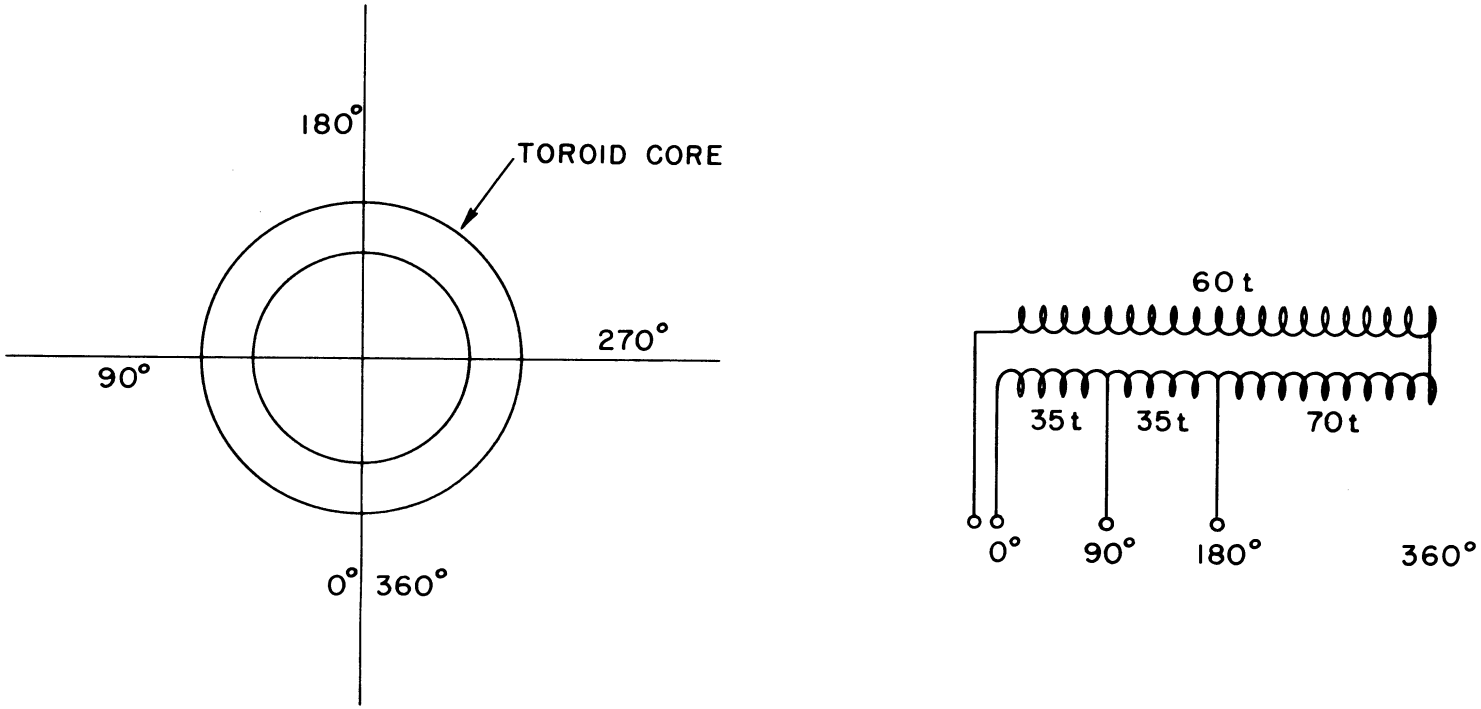

FIG. 8

200 TURN TAPPED TOROIDAL WINDING.

The girdle windings are connected to the integrator-amplifier and its output is displayed on the Y-axis of the scope. An audio signal is fed to the 200-turn winding through a 10,000 ohm resistor.

As in the case of the butterfly loop, one assumes the audio current is constant, and therefore the voltage across the 200-turn winding is proportional to the tangential incremental permeability. This voltage is displayed on the X-axis of the scope.

The envelope of the pattern on the scope is now the tangential incremental permeability as a function of the perpendicular flux density.

4.2 The Basic Ferrospinel Components (D. M. Grimes)

It has long been theoretically realized that internal strains and non-magnetic inclusions could have a large effect upon domain wall movements, and thus the incremental permeability, the losses, and the coercive force. An imperfect, non-uniform region is the reason for non-infinite initial permeability, non-zero losses (at least at low frequencies) and non-zero coercive force. (See reference 2 and other references listed therein.)

Qualitative analysis of the internal strains will be made by X-ray diffraction measurements. The gross magnetostriction of polycrystalline specimens will be measured for the same reason.

The final samples will be analyzed spectrographically by the National Spectrographic Sales Corporation, Cleveland, Ohio. Further analysis will be made to determine the sulphur content. It is necessary to have high-purity oxides to control these factors. Therefore, the following C.P. oxides have been ordered from Harshaw Scientific, Detroit, Michigan:

Fe_2O_3 MnO
ZnO CuO
NiO

to date the ZnO and CuO have been received; both were packed under a Mallinckrodt label. The Fe_2O_3 on hand at present was obtained from Chemistry Stores on campus.

The Li_2CO_3 was obtained from the Lithium Corporation of America, with specifications indicating 99.4% minimum of pure chemical. However, impurities such as glass, straw, and various other materials were found in the salt.

Samples of the CuO, ZnO, and Li_2CO_3 are now in Cleveland for a semi-quantitative analysis.

Efforts are being made to obtain very pure oxides (maximum impurities of 0.02%). If deemed necessary, the very pure metal will be obtained and oxidized here on campus. A study of the necessary techniques for handling materials of this purity is being made.

4.3 The Manufacturing of the Ferrites (D. M. Grimes, L. Thomassen)

4.3.1 Manufacturing Procedure. A typical method of preparing a ferrite is described in reference 3, pp. 344-346. The effect of each procedure in the manufacturing process will be studied.

4.3.2 Manufacturing Equipment

Oven -- Arrangements have been made to use an existing oven for firing the preliminary cores. This oven is not satisfactory for the purposes and will be replaced by a better, more permanent model as soon as possible. The present model has a maximum temperature variation, due to delay time in the thermocouple control, of about 25°. The temperature variation from core to core due to position in the oven would probably be about the same, although no quantitative measurements have been taken. The new model will be designed to have a maximum temperature deviation of about 5°C throughout the oven and about the same deviation due to variation under thermostatic control.

Ball Mill -- A suitable ball mill has been built and is ready for use. Care was taken to prevent any sharp corners in the jar to prevent any oxide sticking. The jar and balls are of cold-rolled steel. Other mixing and grinding devices which would introduce less impurities will be studied.

Die -- A suitable die has been made for toroidal specimens. (See Fig. 9.) Dies for specimens of other shapes will be made as needed.

Press -- A press capable of a total force of 50 tons is available in the department.

4.4 Magnetic and Electrical Measurements

4.4.1 Saturation Magnetization (L. W. Orr, D. M. Grimes). The saturation magnetization will be measured as a function of temperature for the different cores. To do this a G.E. fluxmeter is on order. A refrigerator going to dry-ice temperature and an oven capable of maintaining a temperature of 800°C are being constructed. A cryostat going to still lower temperatures will be constructed.

In addition to the fluxmeter, the 60 cps B-H loop circuit described in Section 4.1 will be used.

4.4.2 Incremental Permeability, Dielectric Constant, Resistivity, and Power Losses in the Core Material (D. M. Grimes, M. H. Winsnes)

4.4.2.1 Resistivity and Dielectric Constant. The dc resistivity will be measured on a Wheatstone Bridge. To measure the ac resistivity, the method described by Polder[5] will be used. To cover up to 40 mc, a General Radio type-716-C capacitance bridge and type-821A Twin-T bridge will be used. To 500 mc, a Hewlitt-Packard type-803A bridge will be used. These readings will also furnish information regarding the complex dielectric constant and thus the "dielectric Q".

4.4.2.2 Incremental Permeability. A bridge circuit is now being designed by Mr. M. H. Winsnes to measure the permeability and Q of the ferrite

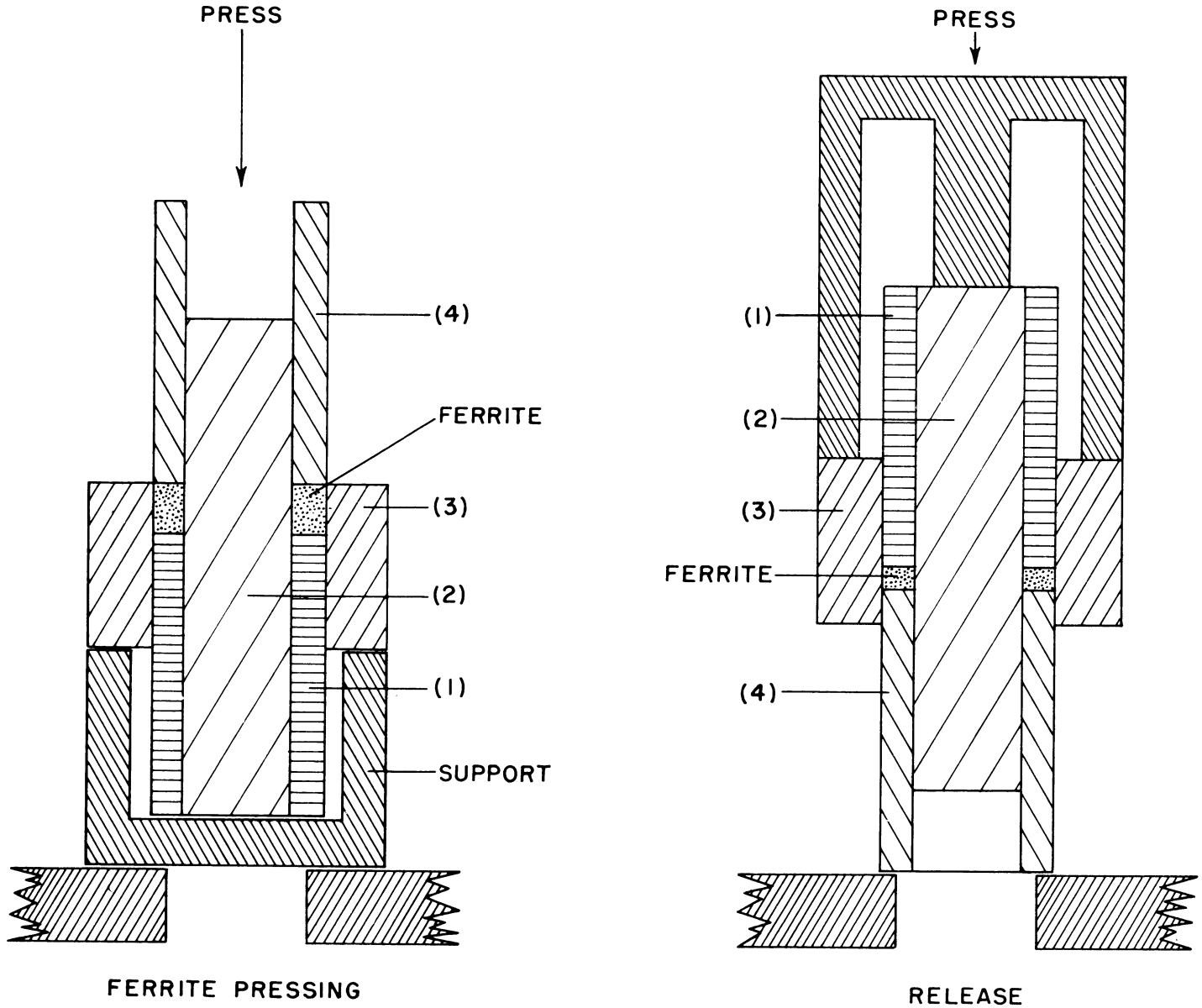

FIG. 9

THE DIE (TO SCALE).

material below a frequency of 400 kc. From 400 kc to 500 mc, the General Radio type-821-A twin-T bridge and the Hewlitt-Packard type-803A VHF bridge will be used. From these measurements the complex permeability can be found, and thus the Q of the core.

4.5 Applicable Physical Measurements

4.5.1 Density. The density will be found by measuring and weighing the core. The increase in density during firing will also be determined.

4.5.2 Magnetostriction. No work was done on magnetostriction during the quarter. A study of experimental methods is being made.

4.5.3 Thermal Expansion Coefficient. No work was done on the thermal expansion coefficient during the quarter. A study of experimental methods is being made.

4.5.4 X-Ray Diffraction (L. Thomassen). A preliminary study was made of a sample of General Ceramics Type-I ferrite. The objective was to find out what the various tools of investigation would show. These tools were: X-ray diffraction in various forms and metallographic polishing and etching. Density measurements and micro-radiography were contemplated but not tried.

Powder picture patterns were made of the sample, using cobalt and chromium radiation with a North American Philips Diffraction unit. The 114 mm diameter camera was used. The crystalline planes were identified. The lattice constant computed was 8.399 Å. No attempt was made to obtain a precision determination or to critically evaluate the ratio of intensities of the lines. It was noted that there were no lines which could not be accounted for, which means that no well-crystallized second phase could be present in concentration over a few per cent. Also, the lines were quite sharp, showing that the material was homogeneous and well-crystallized. If desirable, a quantitative measure of the

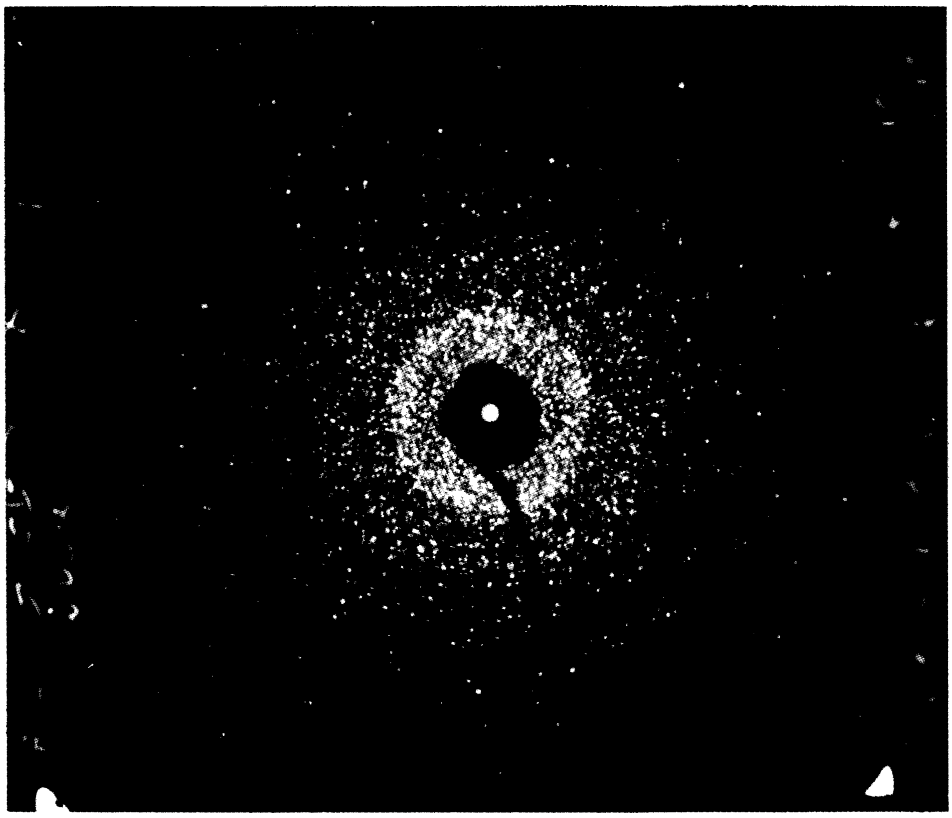

FIG. 10. PINHOLE PICTURE OF FERRITE SAMPLE.
X-RAYS PERPENDICULAR TO AXIS OF TOROID.

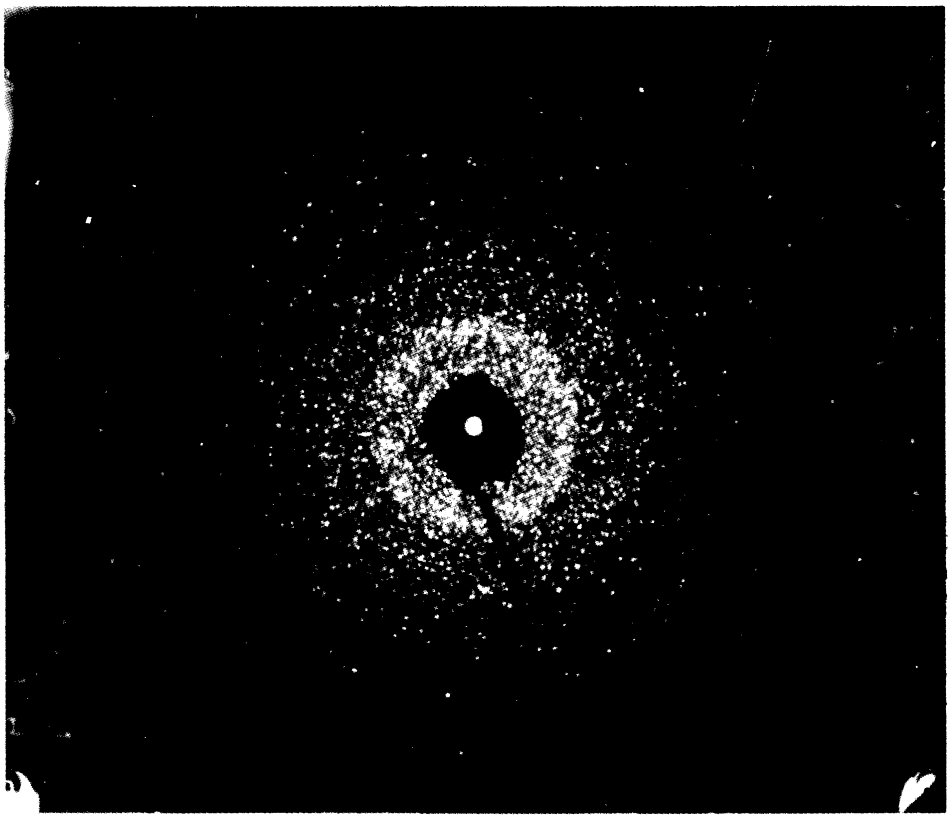

FIG. 11. PINHOLE PICTURE OF FERRITE SAMPLE.
X-RAYS PARALLEL TO AXIS OF TOROID.

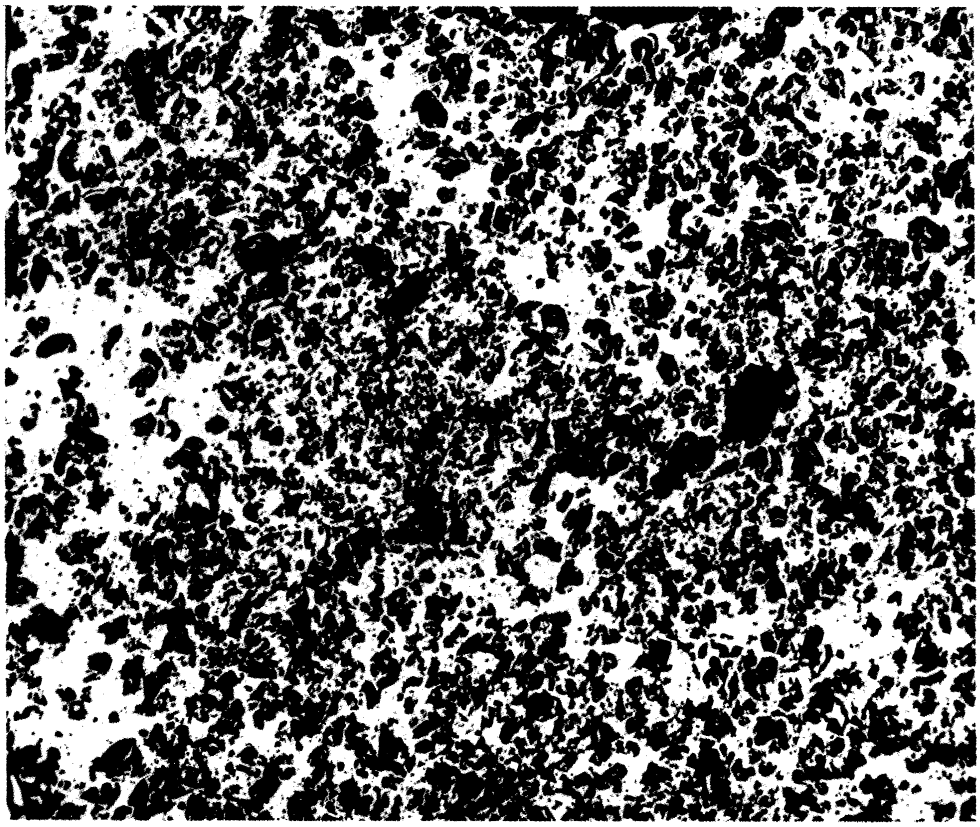

FIG. 12. POLISHED SECTION OF FERRITE SAMPLE
x 100.

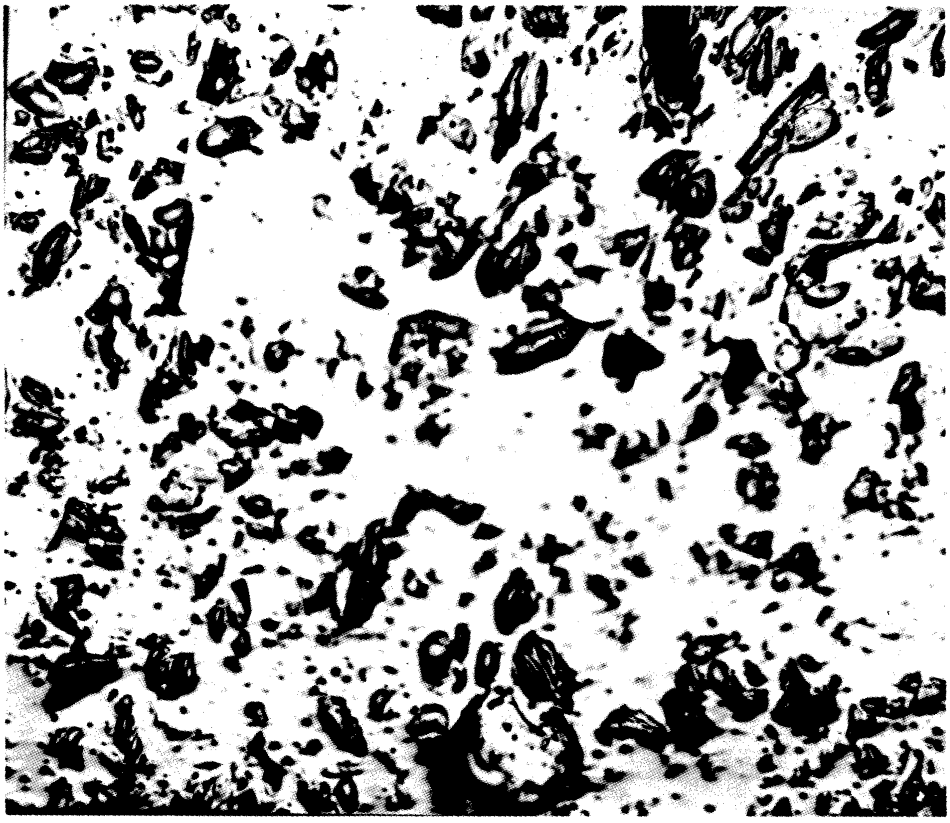

FIG. 13. POLISHED SAMPLE OF FERRITE SAMPLE
x 500.

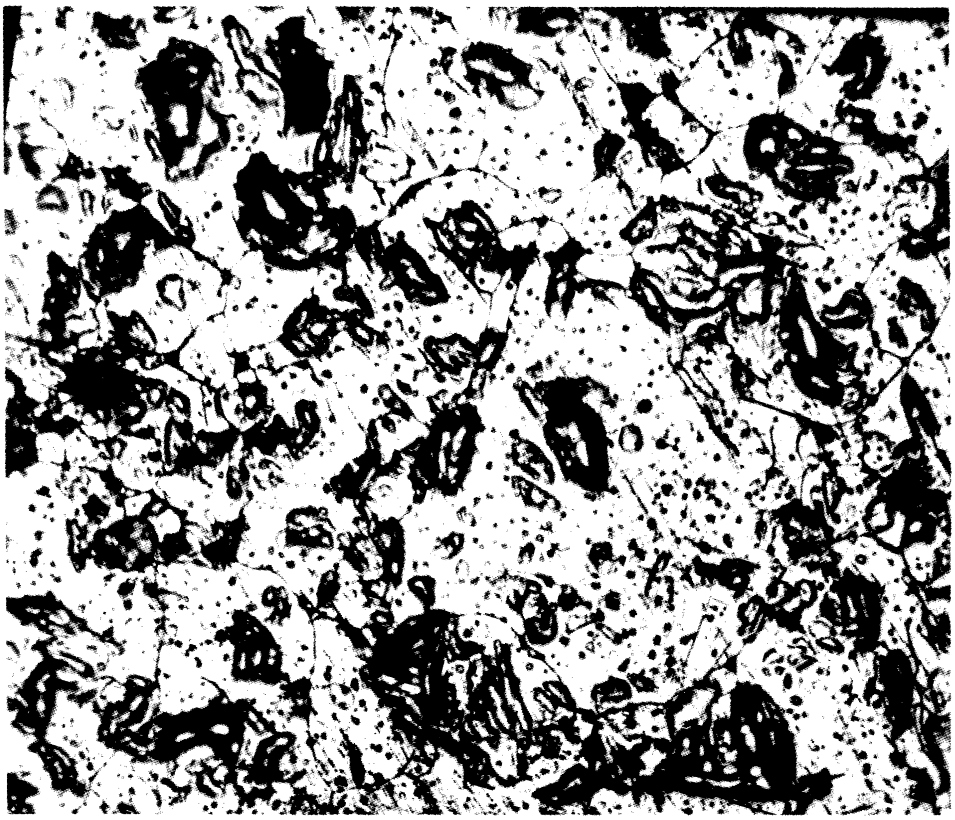

FIG. 14. POLISHED AND ETCHED SAMPLE OF FERRITE x 400.

homogeneity of the ferrites to be made might be obtained by running photometer tracings of the back reflection lines where the resolution is the greatest.

Two pinhole diffraction pictures were made, by shooting a mixture of white and characteristic radiation from a molybdenum target tube through thin sections of the sample. One sample was cut parallel to the axis of the toroid, the other normal to the axis. The pictures are very much alike (see Figs. 10 and 11). They show a great number of spots which are individual reflections from the small crystal grains. Many of the outer spots are arranged on circles with their center in the middle, and are therefore reflections produced by the characteristic radiation. The fact that individual grains reflect the radiation indicates a comparatively coarse structure. Also, there is no bunching of the individual spots on the rings. This would indicate the absence of at least any significant special orientation of the crystals.

4.5.5 Metallographic Polishing (L. Thomassen). Part of the sample was mounted in black bakelite, ground and polished, following the regular metallographic procedures. The structure obtained is shown in Fig. 12. The white material is the oxide, while the black parts of the picture show the voids. The irregular distribution of the void space is quite apparent. The middle of the picture shows several large holes, perhaps even connected with each other, while at the edges of the picture there are larger white areas. Fig. 13 shows the section at 500 x magnification. There are no pronounced shapes, either of the oxide or of the voids, which would indicate the outlines of crystals.

Fig. 14 shows a picture of the etched structure. Strong, hot hydrochloric acid was used as an etching solution. The grain boundaries show up nicely; however, care must be utilized, for after some time, etch pits begin to form within the crystals. It will be seen that the continuous white portions

may contain several grains. The grains seem to be non-uniform in size, and the voids do not all lie in the grain boundaries.

While the metallographic method gives a measure of the grain size, it is not used to find the percentage of voids. The latter could, of course, be found fairly accurately from a density determination.

4.5.6 Curie Temperatures

4.5.6.1 Ferrimagnetic Curie Point (D. M. Grimes). This will be measured on the fluxmeter as part of the program of measuring the saturation magnetization.

4.5.6.2 Antiferromagnetic-Ferrimagnetic Curie Points (E. F. Westrum, Jr). Investigations of the antiferromagnetic behavior of compounds of the actinide elements undertaken by Dr. E. F. Westrum, Jr. and colleagues at the Argonne National Laboratory by means of precision low-temperature heat-capacity measurements indicated that the cryogenic calorimeter may be a powerful ally in the study of the magnetic properties of the ferrite materials. A similar conclusion was reached by Yafet and Kittel,[6] who suggest that the existence of multiple Curie points should most easily be detected by heat-capacity measurements. The use of heat-capacity measurements in this regard avoids the spurious effects in magnetic measurements caused by ferromagnetic impurities, and the anomalies in the heat capacity for typical paramagnetic-antiferromagnetic transitions are well within the range of detection by the cryogenic method.

The initial study to be undertaken in this program is to test the molecular field treatment of the magnetic properties of ferrites given by Yafet and Kittel. In the absence of a reliable sample of composition recommended as promising by Yafet and Kittel (e.g., a mixed zinc-nickel ferrite with less than 30% NiO), the heat capacity of a sample of Ferramic E obtained from the General

Ceramics Company is being measured.

4.5.7 Cryogenic Apparatus (E. F. Westrum, Jr.)

4.5.7.1 The Cryostat. The recently-constructed cryostat for use over the range 4° to 310°K (financed jointly from University funds and those of the Atomic Energy Commission, Research Contract AT(11-1)-70. Project No. 5) is an improved version of one constructed by Westrum, Hatcher, and Osborne,[7] with the essential difference that helium is used as the lowest temperature refrigerant instead of hydrogen, and that a thermal conduction resistance (called the "economizer") is provided. A schematic cross-sectional view of the cryostat employed is provided in Fig. 15. The main outer vacuum can (8) of the cryostat is fixed in place and sealed to the liquid nitrogen trap, the Distillation Products MC-275 Oil Diffusion Pump, and the Welch 1750B Duoseal pump. A thermocouple gauge, an ionization manometer, and an RCA-1949 hydrogen-leak-detection-tube are provided. The entire cryostat assembly is suspended from the head plate (21) and is lifted by the support rods and ring with a block and tackle and clamped at a convenient height for assembly, etc. The only vacuum joint broken is that between the head plate and outer can; this is sealed with an O-ring (22).

The calorimeter assembly is suspended by a knot at the end of a piece of 18-pound braided silk flycasting line (24), which is attached to the windlass shaft (19); the electrical leads, which are suspended in a helix from the adiabatic shield (16), are the only other conducting path to it during measurements. The adiabatic shield is of chromium-plated copper; the top plate is soldered into place; and the bottom is held in tight thermal contact by small screws. The joints are slightly tapered, and Lubriseal grease is used to improve thermal contact. The cylindrical portion of the shield has a helical depression in which all of the leads are laid beneath the heater windings for thermal tie-down; the heater

windings are bifilarly wound of double glass-covered Advance wire and cover practically the entire outer surfaces of all parts of the shield.

The shield is supported from the ring (25) by three strands of braided silk cord, and the lead wires are again formed into a helix in this region. During the process of cooling the calorimeter to low temperatures, the calorimeter (26) is simply drawn upward by turning the windlass. The carefully-machined cone on the calorimeter engages the bottom cone on the adiabatic shield and also draws the shield upward so that its upper cone engages that on the bottom of the helium tank (14). The position of the calorimeter is indicated by the pointer-indicator hanging on a cord from the windlass shaft. A coil spring in the calorimeter suspension cord prevents inadvertent excess tension from breaking the cord. A ring (25) provided with a difference thermocouple and an independent heater permits the reduction of the temperature gradient along the bundle of leads and thus facilitates shield control.

The helium (17) and nitrogen (13) radiation shields are constructed of 0.032 in thick copper, bright chromium-plated inside and out, and are attached to the bottom of their respective tanks. The helium tank (14) has a total weight of 1.23 kg and a volume of 1880 cc, and is supported both by the helium exit tube as well as by silk cords to the "economizer" (12). The "economizer" is in turn supported by nylon cords from the nitrogen tank as well as by the helium exit tube. The economizer was designed to reject heat to the effluent helium gas, thereby maintaining it at some temperature lower than the temperature of the nitrogen tank, thus reducing conduction along the leads and connecting tubes to the helium system. Approximate tests indicate that the present economizer reduces the loss of helium at temperature equilibrium by about 75%. The nitrogen tank (14) (weight = 5.67 kg, volume = 2700 cc) is supported by wire loops from the top

support of the outer, essentially isolated radiation shield (9) as well as by its filling tube (3) and the helium filling tube radiation shield. The nitrogen inlet (3) is simply closed with a rubber stopper. The side tube is connected either with the atmosphere or a high-capacity, mechanical vacuum pump.

The helium filling or transfer tube (2) makes contact with its surrounding jacket only at the inlet end. Screw fittings (7) facilitate the closure of the inlet end, or the extension of it, by approximately 20 more inches to reach the bottom of the vessel from which helium is being transferred. The outlet connection leads to a manifold arranged so that exit helium may be metered through a wet test meter, discarded to the atmosphere, or tank helium under pressure purged through the helium system.

The general operation of the cryostat depends on the temperature range in which it is desired to work; above 90°K both nitrogen and helium tanks are filled with liquid nitrogen. In the range 52°K to 90°K the liquid nitrogen in the helium tank is evacuated until the nitrogen solidifies. For operations in the range 4°K to 60°K the helium tank is filled with liquid helium after precooling with solid nitrogen, and the liquid nitrogen in the nitrogen tank is evacuated until it solidifies. A special heating coil wound about the bottom end of the helium tank facilitates the removal of excess precooling solid nitrogen. Approximately 300 cc of liquid helium are required to cool the helium tank from 60°K to 4°K, an additional 300 ml to 700 ml are required to cool the adiabatic shield, calorimeter, and sample; so that 1 to 1.5 liters of liquid helium suffice for a typical series of measurements in the liquid helium region. The loss rate of liquid helium with the system completely cooled is about 11 cc of liquid helium per hour.

4.5.7.2 The Calorimeter. The gold-plated copper calorimeter (Laboratory Designation W-5), 3.8 cm in diameter and 7.7 cm long, is shown in

schematic section in Fig. 16. The thickness of the shell is 0.4 mm. Eight vanes of 0.1 mm copper foil aid in establishing temperature equilibrium. A reentrant well contains a platinum capsule-type thermometer[9] (manufactured by Leeds and Northrup Company, and calibrated by the National Bureau of Standards) within a cylindrical copper heater tube carrying 160 ohms of B. and S. No. 40-guage Advance (constantan) double fiberglass insulated wire, which is wound bifilarly in double-threaded grooves and cemented in place with Formvar. The glass head through which the thermometer leads are sealed is entirely within the enlarged portion of the well, and the lead wires to both the thermometer and the heater are brought to temperature equilibrium with the outside of the calorimeter by means of a small copper spool around which the leads are wound and cemented with Formvar, and a cover bolted into place with 00-90 brass hexagonal cap screws. An enameled differential thermocouple junction makes a snug fit in a small tube soldered to the calorimeter. Weighed amounts of Lubriseal stopcock grease are used to establish thermal contact between thermometer, heater, spool, thermocouple, and calorimeter. Pure helium gas at a pressure of one atmosphere at 25°C is used to provide thermal conductivity between the sample and the calorimeter. After weighing in the sample and Cerraseal soldering on the cover, the calorimeter is evacuated and the helium added through a small hole drilled in the top of a thin-walled monel stud, while the calorimeter is in a vessel on a vacuum line, and then the hole is quickly closed with Cerraseal solder while all but the top of the calorimeter is immersed in water. The amounts of solder and stopcock grease were carefully adjusted to be the same within less than 0.2 mg in the measurements on the empty and full calorimeter. The mass of the entire empty calorimeter, including thermometer, heater, spool, and grease, is 82 grams.

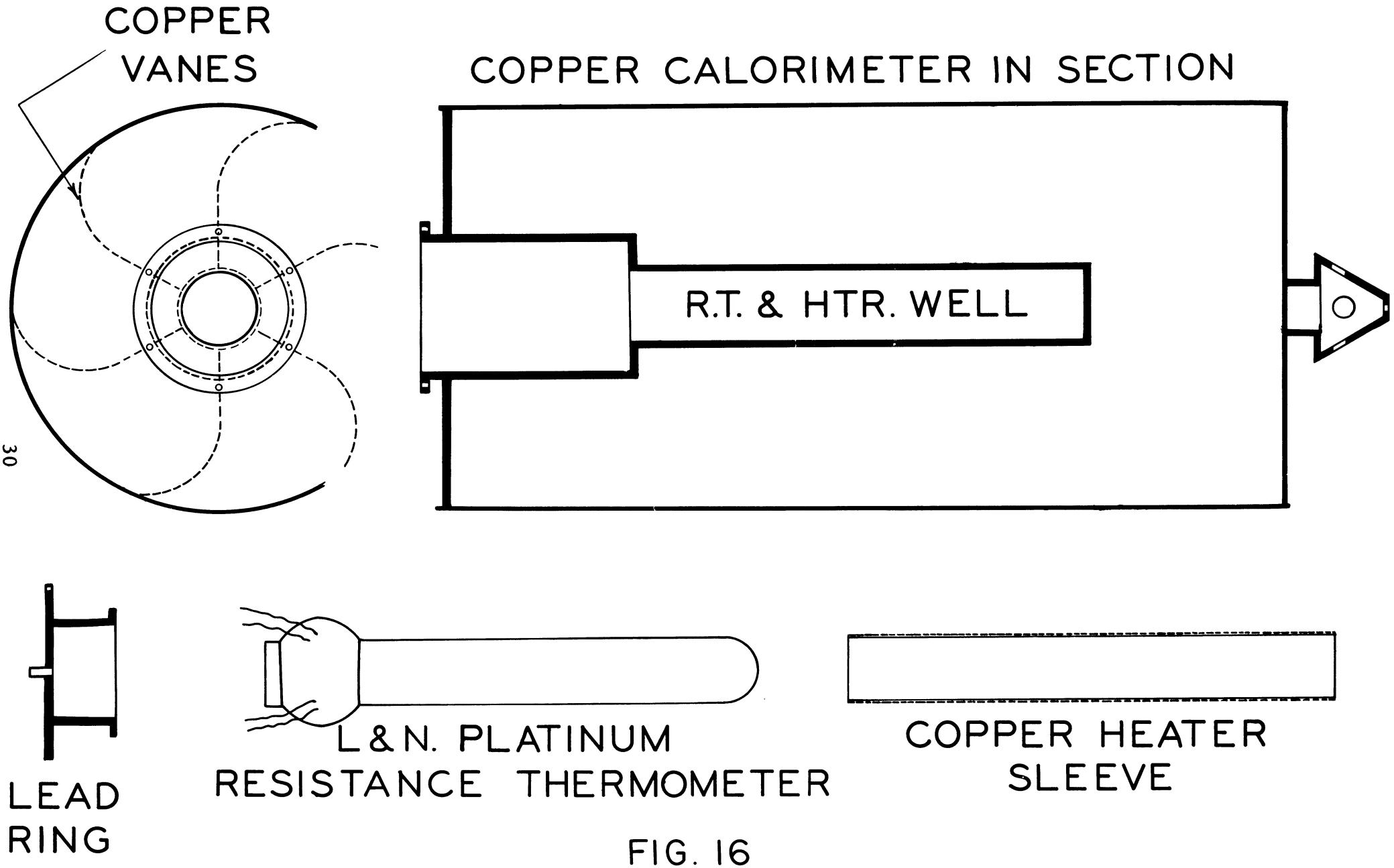

FIG. 16

THE CALORIMETER

4.5.7.3 Electrical Circuits. The copper-constantan thermocouples for controlling the adiabatic shields were connected through selector switches to two galvanometers with working sensitivities of 0.01 μv/mm. One galvanometer was used to read the temperature difference between the calorimeter and the top, middle, or bottom of the shield, and the other was used to read the temperature difference between the middle of the shield and the ring. The three ring and shield heaters were supplied with alternating current controlled by variable voltage transformers and variable resistor circuits.

The current and the potential drop in the resistance thermometer and in the heater were measured with an autocalibrated White double potentiometer, a galvanometer with a working sensitivity of 0.04 μv/mm, calibrated resistors, and an unsaturated Weston standard cell. Both the resistance standard and the standard cell were calibrated by the National Bureau of Standards. An electric timer operated by a calibrated tuning fork and amplifier was automatically started at the beginning of the energy input and stopped at the end. A thermometer current of 4 ma was used up to about 60°K and 2 ma was used at higher temperatures.

4.5.7.4 Method of Operation. The virtually zero temperature drift of the calorimeter is observed for 10 to 15 minutes; then electrical energy is added for a measured period of 5 to 10 minutes; and finally the drift is observed for at least 15 minutes. Usually the drift becomes constant about 5 minutes after the end of the energy input. The observed drifts are used to extrapolate the initial and final temperatures to the mid-point of the energy input and thus to correct for the combined effects of heat interchange with the inner shield and the thermometer current.

One operator observes the electromotive forces of the differential thermocouples and adjusts the current to the shield heaters to maintain the small

constant temperature differential between the shield and the calorimeter and to maintain the ring several tenths of a degree colder. The temperature differential between the shield and the calorimeter is generally controlled to within 0.002°C except for a few seconds at the start and finish of the energy input. A second operator measures the temperature and energy with the White potentiometer.

The heat capacity of the calorimeter filled with helium has been determined. The measurement of the apparent heat capacity of the calorimeter plus the ferrite sample and helium is in progress at present. From these data and suitable corrections, the true heat capacity of the ferrite sample will be obtained and examined for thermal anomalies.

4.5.8 Measurement of the Hall Effect in Ferrites (B. Hershenov, E. Katz). Pugh, et al.,[10] suggested a semi-empirical formula for the dependence of Hall effect upon the field H and the magnetization M.

$$E_H = R_o H + R_1 M$$

where R_o is the ordinary Hall coefficient and R_1 is the extraordinary coefficient and E_H is the Hall emf. The ordinary effect is proportional to H and the extraordinary effect is proportional to M and is predominant at low fields.

Foner's[11] preliminary results on nickel ferrites indicate that this relationship for ferromagnetic substances holds true for nickel ferrites.

The applicability of the above relationship for other ferrites will be checked at the same time that the Hall mobility is determined.

Fig. 17 (see reference 14) is a block diagram representation of the apparatus* to be used in measuring the Hall emf in ferrites, subject to the revisions mentioned in this report. The Hall mobility is then determined by the

*The apparatus was designed by John L. Levy under the supervision of Prof. E. Katz. The work was sponsored by O.N.R., U.S. Navy Department Contract No. NONR-154(00), Project No. 017416 (see reference 14).

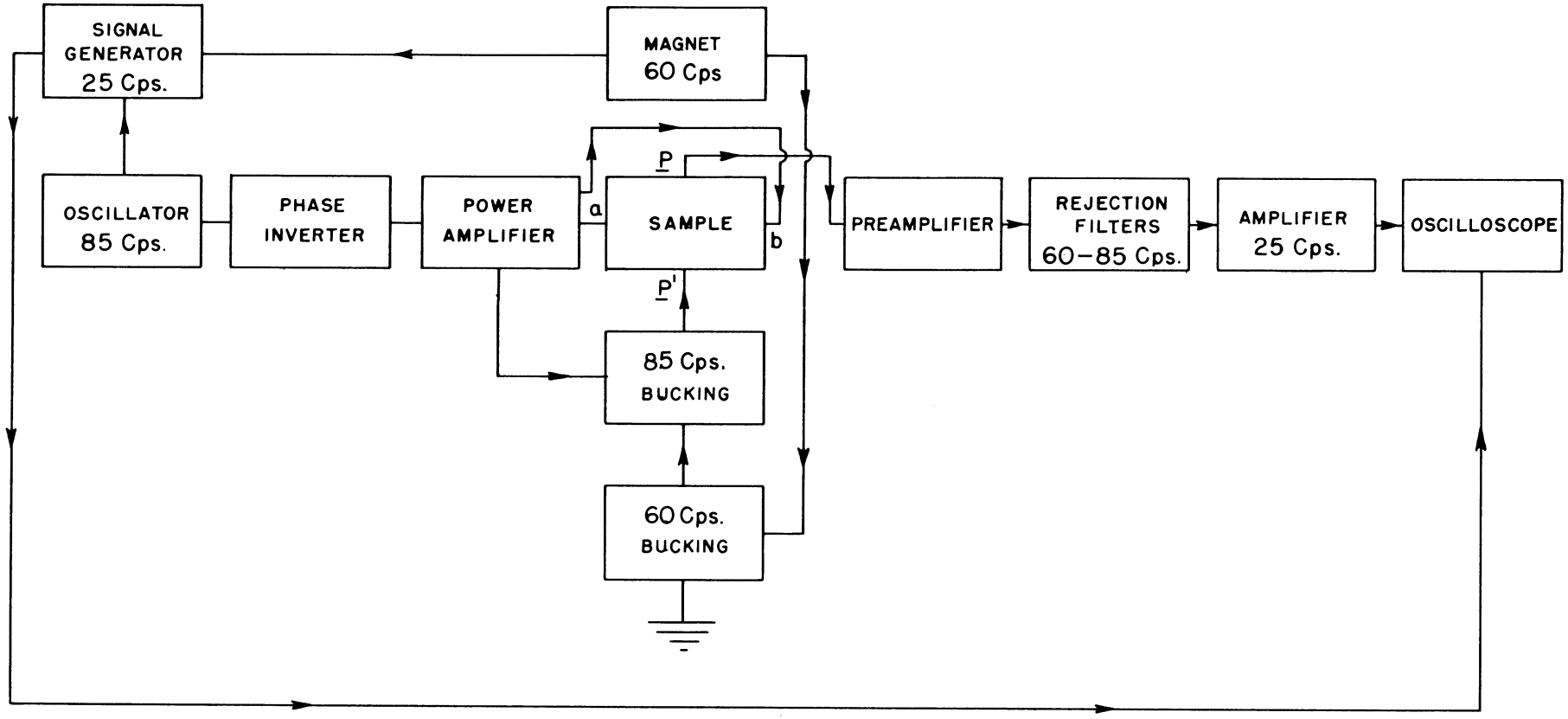

BLOCK DIAGRAM OF THE HALL COEFFICIENT APPARATUS.

FIG. 17

relation,

$$E_H = \mu_H EBK$$

or in terms of the electric potential,

$$V_H = \mu_H VB \frac{w}{\ell} K$$

where ;

E_H = Hall electric field intensity across width of specimen

μ_H = Hall mobility

E = Electric field intensity applied across length of specimen

B = Flux density. The magnetic field is applied perpendicular to the plane determined by the length and width of the specimen.

w = Width of the specimen between the Hall electrodes

ℓ = Length of the specimen

K = Geometry correction factor for shunting effect of current contact across the ends of the specimen.

The apparatus operates with alternating electric and magnetic fields of two different frequencies f_1 and f_2. The Hall field then consists of two components of equal amplitude with frequencies $f_3 = f_1 - f_2$ and $f_4 = f_1 + f_2$. We then have

$$E_H = \mu_H EB = \frac{\mu E_o B_o}{2} \left\{ \cos \left[2\pi(f_1 - f_2)\, t - \phi \right] + \cos \left[2\pi(f_1 + f_2)\, t + \phi \right] \right\}$$

where

$$E = E_o \sin 2\pi f_1 t$$

$$B = B_o \sin (2\pi f_2 t + \phi)$$

The frequency of the magnetic field is chosen equal to 60 cps, the frequency of the power line. The frequency f_3, the Hall signal frequency to be detected, should be low to insure a high input impedance for the detector stage, namely, the preamplifier, filtering network, and amplifier, since ferrites

generally exhibit a high resistivity. Furthermore, the lower the amplifier frequency, the narrower its possible bandwidth Δf, and the higher the signal-to-noise ratio of the detector. It is not advantageous, however, to choose too low a frequency for the following reasons:

a. Noise due to microphonics and flicker effect increases at low frequencies.

b. Δf should not be reduced excessively because of the drift of f_1 and f_2. The response time of the amplifier, which is proportional to $\frac{1}{\Delta f}$, should not exceed a few seconds, allowing measurement to be made in a time short enough to avoid excessive drift voltage at the Hall electrode.

c. If f_3 is too low, f_1 is close to f_2, and a signal generator tuned at f_1 will tend to drift toward f_2 under electromagnetic pick-up from the power-line circuits.

Consequently, in contrast to Russel and Whalig's[12] choice of a 10 cps Hall signal, a value of f_3 = 25 cps has been chosen. This is midway between the two subharmonics of f_2 and permits the best rejection of these signals if they are picked up in the Hall circuit. This leaves a choice of f_1 = 85 cps or f_1 = 35 cps. The first value is used because construction of the driving system is easier at this higher frequency, and it is more readily rejected by the selective detector than the 35 cps which is close to the 25 cps Hall signal to be passed by the amplifier.

4.5.9 Description of Apparatus for Measurement of Hall Effect

4.5.9.1 Driving Stage. The source of the primary electric field consists of a stable harmonic oscillator tuned at 85 cps, a tuned phase-inverter, and a power amplifier.

a. The 85 cps oscillator consists of two resistance amplifier stages tuned and brought into oscillation by a Wien bridge in the feedback loop.

The output of the oscillator is about 10 volts rms and is controlled by a variable resistor in the feedback circuit.

b. The phase inverter consists of two resistance amplifier stages tuned by a twin-T filter inserted in the feedback circuit of each tube.

c. The power amplifier is a push-pull power amplifier with two "5881" tubes in parallel on each side. This allows considerable mismatch with little distortion. All the available power is not generally used. The output transformer has adjustable turns ratio to allow an approximate impedance match of sample and amplifier output.

4.5.9.2 The Detection Circuit. The detecting circuit consists of a pre-amplifier, filtering network, and an amplifier.

a. The pre-amplifier consists of a starved pentode stage directly coupled to a triode resistance amplifier stage. Filament and plate voltage is supplied by batteries to eliminate 60 cps pickup from electronic power supplies and mixing of 60 and 85 cps signals. A 25 cps twin-T filter is in the negative feedback loop around the two stages.

b. The filtering section consists of 60 cps and 85 cps twin-T rejection filters.

c. The amplifier is composed of two identical pentode stages tuned at 25 cps and separated by a triode buffer amplifier.

The gain of the complete detecting system is 4.5×10^4 at 25 cps, 20 at 60 cps, and 200 at 85 cps with a bandwidth of .7 cps at 25 cps.

4.5.9.3 Bucking Section. The bucking section generates 60 cps and 85 cps signals with adjustable amplitude and phase. The phase-shifting circuit consists of a sine-cosine resolver loaded with an rc circuit. The phase shift is directly proportional to the angle between the rotor and stator. The 85 cps input signal is provided by a transformer in parallel with the output

transformer of the power amplifier. The 60 cps input is obtained from a pickup coil on the back leg of the magnetic core.

This procedure allows the 85 and 60 cps bucking signals to follow the fluctuations of the primary electric field and magnetic field respectively.

4.5.9.4 25 CPS Signal Generator. This is generated by mixing an 85 cps signal from the oscillator of the driver stage with a 60 cps signal from the ac magnet. The cross modulation component of the mixer output is selected and amplified by a 25 cps tuned amplifier similar to the amplifier of the detecting system. The output is used to determine the phase of the Hall signal, and therefore the sign of the Hall mobility, by comparing the Lissajous figure with that of a known specimen.

4.5.9.5 AC Magnet. This magnet produces the 60 cps magnetic field. Its pole faces are 5 x 9 cms with an air gap of about 3.5 cms. The pole pieces are truncated along their entire height. The linear relationship between B and excitation current I holds up to a flux density of about 0.9 Webers/m^2. At higher field intensities the reluctance of the magnetic core becomes appreciable, and the third harmonic distortion appears in the waveshape of the magnetic field.

4.5.9.6 Possible Revisions. The spectral density of the noise, if it is due to thermal fluctuations with a high relaxation time, should decrease at higher frequencies. If this is the case, the advantages of a low Hall signal frequency would be overshadowed by a lower current noise. It would be better to measure the second component of the Hall signal--the frequency f_4 = 145 cps. For the selective amplifier, this involves the replacement of the 25 cps twin-T by similar 145 cps filters. If this modification keeps the "Q" of the detecting circuit at its present value, Δf would be larger and would offset the gain due to a lower spectral noise density. Δf could be narrowed again by adding a

phase-sensitive detector to the present selective amplifier. If the reference signal is provided by a mixer analogous to the 25 cps signal generator of the present set-up, then the circuit described by Shuster[13] would be well suited. This procedure would allow the simultaneous determination of amplitude and phase of the Hall signal as well as a statistical analysis of the detection system output in case of weak Hall signals.

4.5.10 Microwave Studies at Over 500 MC. No work was done during the quarter. An investigation of the problems in this area will be undertaken by Dr. H. W. Welch, Jr.

4.5.11 Thermal Conductivity. No work was done during the quarter. Results of such measurements will be useful in heat capacity measurements and in determining the temperature stability of tuning units.

5. CONCLUSIONS (D. M. Grimes)

This first quarter's work was primarily concerned with the organization of the program, getting together the appropriate personnel, ordering equipment, and making decisions regarding the course of the future work.

6. PROGRAM FOR THE NEXT INTERVAL (D. M. Grimes)

6.1 Reversible Susceptibility

If the necessary equipment arrives in time, the experimental data necessary for a check of the theory of reference 1 will be gathered during the quarter.

6.2 Oxide Purity

A decision will be made regarding the degree of purity which will be the ultimate goal.

6.3 Core Manufacturing Equipment

The firing oven with the characteristics desired will be designed. A cryostat to go to liquid nitrogen temperatures will be designed; the moderate temperature oven and the refrigerator to dry ice temperature should be completed.

A decision regarding the binder to be used must be made. This will depend, in large measure, upon the choice of manufacturing technique.

6.4 Measurement of Magnetic and Electrical Properties

Satisfactory equipment is either available or on order for all necessary measurements except the permeability and the coil Q below 400 kc. Further work will be done to get a better method for doing this.

As soon as the equipment now on order arrives, measurements can be started on the other properties. Temporarily, the circuit mentioned in Section 4.4.3.2 will be used for the low frequency permeability and Q measurements.

6.5 Applicable Physical Measurements

In addition to the measurements described as being worked on under Section 4.5, work will be started on the magnetostriction coefficient and the thermal coefficient of expansion as soon as possible.

REFERENCES

1. Grimes, D. M., "Theory of Reversible Magnetic Susceptibility with Application to Ferrites," Technical Report No. 8, EDG, University of Michigan, August, 1952.

2. Kittel, C., "Physical Theory of Ferromagnetic Domains," Rev. Mod. Phys., 21, pp. 541-582, 1949.

3. Harvey, R. L., Hegyi, I. J., Leverenz, H. W., "Ferromagnetic Spinels for Radio Frequencies," RCA Review, 11, No. 3, pp. 321-363, 1950.

4. Orr, L. W., "Permeability Measurements in Magnetic Ferrites," Technical Report No. 9, EDG, University of Michigan, September, 1952.

5. Polder, D., "Ferrite Materials," Inst. E.E., 97, Part 2, pp. 246-256, 1950.

6. Kittel, C. and Yafet, Y., "Antiferromagnetic Arrangements in Ferrites," Phys. Rev., 87, pp. 290-294, 1952.

7. Hatcher, J. B., Osborne, D. W., Westrum, E. F., Jr., "The Entropy and Low Temperature Heat Capacity of Neptunium Dioxide," Argonne National Laboratory Report ANL-4808, April, 1952. (To appear in J. Chem. Phys., March, 1953).

8. Huffman, H. M., "Low Temperature Calorimetry at the Bartlesville Station of the Bureau of Mines," Chem. Rev., 40, p. 1, 1947.

9. Hoge, H. J. and Brickvedde, F. G., "Establishment of a Temperature Scale for Calibration of Thermometers Between 14° and 83°K," N.B.S. Jour. of Research, 22, p. 351, 1939.

10. Pugh, E. M., Rostoker, N., Schindler, A., "On the Hall Effect in Ferromagnetics," Phys. Rev., 80, p. 688, 1950.

11. Foner, S., "The Hall Effect in Nickel Ferrite," Phys. Rev., 88, p. 955, 1952.

12. Russel, B. R. and Whalig, C., "A New Method for Measurement of Hall Coefficient," Rev. Sci. Inst., 21, p. 1028, 1950.

13. Schuster, N. A., "A Phase Sensitive Detector Circuit Having High Balance Stability," Rev. Sci. Inst., 22, p. 254, 1951.

14. Levy, John L., "An Experimental Upper Limit for the Magnitude of the Hall Effect in Single Crystals of Sodium Chloride," Thesis, University of Michigan, 1953.

DISTRIBUTION LIST

Copy No. 1	Director, Electronic Research Laboratory Stanford University Stanford, California Attn: Dean Fred Terman
Copy No. 2	Commanding Officer Signal Corps Electronic Warfare Center Fort Monmouth, New Jersey
Copy No. 3	Chief, Engineering and Technical Division Office of the Chief Signal Officer Department of the Army Washington 25, D. C. Attn: SIGGE-C
Copy No. 4	Chief, Plans and Operations Division Office of the Chief Signal Officer Department of the Army Washington 25, D. C. Attn: SIGOP-5
Copy No. 5	Countermeasures Laboratory Gilfillan Brothers, Inc. 1815 Venice Blvd. Los Angeles 6, California
Copy No. 6	Commanding Officer White Sands Signal Corps Agency White Sands Proving Ground Las Cruces, New Mexico Attn: SIGWS-CM
Copy Nos. 7-81	Transportation Officer, SCEL Evans Signal Laboratory Building No. 42, Belmar, New Jersey For - Signal Property Officer Inspect at Destination File No. 25052-PH-51-91(1443)
Copy No. 82	W. G. Dow, Professor Department of Electrical Engineering University of Michigan Ann Arbor, Michigan
Copy No. 83	H. W. Welch, Jr. Engineering Research Institute University of Michigan Ann Arbor, Michigan

Copy No. 84	Document Room Willow Run Research Center University of Michigan Willow Run, Michigan
Copy Nos. 85-94	Electronic Defense Group Project File University of Michigan Ann Arbor, Michigan
Copy No. 95	Engineering Research Institute Project File University of Michigan Ann Arbor, Michigan